Underwater 3D printing of cement-based mortar

B. Mazhoud, A. Perrot, V. Picandet, Damien Rangeard, E. Courteille

UNDERWATER 3D PRINTING OF CEMENT-BASED MORTAR

Brahim MAZHOUD [a*], Arnaud PERROT [a], Vincent PICANDET [a], Damien Rangeard [b], Eric Courteille [b]

[a] Univ. Bretagne Sud, UMR CNRS 6027, IRDL, F-56100 Lorient, France

[b] INSA Rennes - EA 3913, LGCGM, F-35000 Rennes, France

Postal address: UBS – IRDL, Centre de Recherche C. Huyghens – BP 92116 – 56321 LORIENT– France

brahim.mazhoud@univ-ubs.fr

arnaud.perrot@univ-ubs.fr

vincent.picandet@univ-ubs.fr

damien.rangeard@insa-rennes.fr

eric. Courteille @ insa-rennes.fr

* Corresponding author: Tel: +33.2.97.87.45.77, Fax: +33.2.97.87.45.72

Abstract

Nowadays, the development of renewable marine energies and needs for coastal protection to face global warming issues goes simultaneously with the fast development of digitally based construction methods such as concrete 3D printing. This creates the conditions to change the coastal and off-shore construction methods. Therefore in this study, we assess the possibility to design an underwater 3D printing materials. This possibility needs to develop cement-based materials that are simultaneously printable (pumpability, fast structuring) and also resistant to water washing out. After a mix design protocol that complies with the rheological requirements of the concrete and its water anti-washout properties (through permeability measurements), 3D printed samples has been fabricated in air and underwater. Then, the compressive strength of hardened printed mortar has been measured in order to validate the concept of the process.

Keywords: Cement-based material; Rheology; Anti-washout admixture; 3D printing.

1. Introduction

Concrete 3D printing technologies have received significant attention in the construction industry. Especially, extrusion-based methods seems to be the most advanced technology [1–5]. The potential benefits of this technique are various [6,7]: time and cost reduction, quality and safety improvement, reduction of environmental impact by using topology optimization and fabrication of multi-functionalities elements by taking advantage of complex geometries [8].

In the extrusion 3D printing methods, layers of cement-based are successively deposited by a robotic arm to fabricate construction elements or a whole structure. Many researchers have reported that the stability of the structure under printing can be described as a competition between the structural build-up rate of the cement-based material and the rate of increase of the load acting on the structure due to its increasing height [5,9]: This means that the mortar must have gained sufficient strength to withstand the vertical load generated by the subsequently printed materials [10]. It is important to note that structural build-up of cement-based materials is also involved in other building process such as self-compacting concrete formwork pressure, multilayer casting,... [11–16].

The ability of the deposited layers to sustain its own weight is linked to its rheology (and its evolution in time) and more particularly to both yield stress and elastic modulus [3,17]. During the layer by layer building of a wall, the first deposited layer undergoes the heaviest load. In order to ensure the wall stability during the process, the yield stress of the cement-based material must be high enough to sustain this load. Here, a paradox appears: the mortar must be sufficiently fluid for pumping and extrusion flow but at the same time strong enough to ensure the stability of the structure. The structural build-up of the deposited concrete can here beneficially use to allow for the mix-design of a material that is fluid during extrusion and sufficiently rigid after being left at rest after deposit. Structural build-up of the cement-based materials leads to an increase of the macroscopic yield stress over resting time [18–22]; this mechanical strengthening is mainly due to CSH bridges created at the contact points between cement particles (nucleation) and appears before cement setting time (so-called “dormant period”) [23]. For ordinary Portland cement, the yield stress of cementitious materials linearly increases during the first hour of rest [19]. After this first

50 linear evolution, Perrot et al. have developed a model that describes an exponential increase of the yield
51 stress. Another reason of concrete 3D printing failure can be due to self-bucking especially when the printed
52 shape has high slenderness. In this case, the elastic properties of the sample are crucial [20,24].

53 Nowadays, the development of marine energies and new means of production based on the technique of
54 3D printing can influence off-shore construction methods. The idea of using, in place, underwater additive
55 manufacturing, where the effect of gravity is decreased and the greater freedom of form, seems attractive.
56 This technique could be used not only for the implementation of anchors and foundation systems, for the
57 maintenance of submerged structures but also for the building of artificial reefs, a mandatory compensatory
58 measure for setting up marine energy plants. This last problem really seems to be able to find an answer in
59 the development of underwater 3D printing. Indeed, the preservation of marine biodiversity is both an
60 environmental emergency (maintaining sufficient fish stocks for fishing) and an economic one.

61 According to a survey on literature dealing with concrete 3D printing, no study has been reported on the
62 possibility to print concrete elements directly underwater. Therefore, the main objective of this study is to
63 show that it is possible to print concrete underwater. To achieve this objective, anti-washout admixture
64 (AWA) has been added to cement mortar in order to decrease the permeability of the cement mortar in the
65 fresh state. Hence, special care has to be given to the mix-design of a formulation having high washout
66 resistance [25,26]. In fact, the permeability of the fresh-state cement mortar must be adjusted to prevent
67 surrounding water to intermix with the fresh mortar in the case of printing in submerged conditions. Indeed
68 Assaad and Issa [27] have shown that the reduction of the permeability of the underwater concrete in the
69 fresh state reduce the washout loss.

70 Firstly, the influence of water to cement mass ratio (W/C) and AWA content on yield stress (and its
71 evolution with time) and elastic modulus of the studied mortars will be assessed in order to evaluate and
72 predict the so-called buildability if the tested materials. High yield stress will prevent the structure to
73 collapse due to the weight of the printed structures and is also representative of the interparticle forces at
74 microscale [28–30]. This means that high yield stress provides stronger bond between cement particles and
75 thus prevent washout. High elastic modulus will prevent the buckling of the structure during printing.

In addition, permeability measurements were used to quantify the effect of W/C and AWA content on the cementitious material permeability (in the sense of hydraulic conductivity). For that purpose, a constant water head device for permeability measurement dedicated to cement-based materials and developed by Picandet et al. [31] and validated in other studies [32–34] has been successfully used. Low permeability will be representative of a dense microstructure that will be more accessible to the water outside the material.

Finally, 3D printing of mortar carried out underwater or not and at different printing head speeds, are presented and the subsequent mechanical properties (compressive strength) of the printed elements are measured.

2. Materials and methods

2.1. Binder

An ordinary Portland Cement (CEM 1 52.5N) with particle size distribution ranging between 0.1 and 100 µm with a mean grain diameter of approximately 15 µm and specific density of 3.15 is used. Its specific surface estimated with Blaine device is 3390 cm^2/g. According to Vicat needle test, The initial setting time of the cement is 90 minutes and the final one is 245 minutes. River sand 0/2, with a density of 2600 kg/m^3 and coming from Britanny is added to the tested mortar. In order to prevent the presence of large sand particles with diameter greater that can lead to pumping and extrusion blockage, the sand was sieved by means of a sieve of mesh 1 mm before use. The limestone filler used in this work has grain size ranging from 0.1 to 100 µm (d50 = 15 µm).

In order to mix-design printable mortar, the superplasticizer was added to the formulation. It is a commercial polycarboxylate superplasticizer containing 20% of dry polymer. In this study, a single dosage of 3 % in mass of cement was chosen (maximum recommended dosage with a polymer dry extract over cement equal to 0.6%)). The superplasticizer was added to the mixing water. Such dosage provides the best

dispersion of the cement particles. Consequently, pore size are smaller and then the permeability of the mortar is reduced as shown by Perrot et al. [33].

The anti-washout admixture used in this study is a commercial white powdered admixture for concretes dedicated to deep structures. The main active molecules of this product is cellulose ether. It makes it possible, in particular, to ensure the cohesion and homogeneity of the concrete during casting and to counteract the phenomena of segregation and / or phase separation. It also promotes the stability of concrete during pumping. The AWA powder is first mixed with dry elements. The dosage of AWA is given as the AWA to cement mass ratio.

The different ratios and mix compositions are summarized in Table 1. For all the formulations the ratio SP/C was kept fixed to 0.03.

Table 1: Mass ratios of the components of different studied cement mortar

Formulations	Ratio			Percentage (%)		
	AWA/C	W/C	SP/C	Cement	Sand	limestone filler
M1_0.38_3%SP_0.5%AWA	0.005	0.38	0.03	32.5	50.0	17.5
M1_0.39_3%SP_0.5%AWA		0.39		32.5	50.0	17.5
M1_0.40_3%SP_0.5%AWA		0.40		32.5	50.0	17.5
M1_0.42_3%SP_0.5%AWA		0.42		32.5	50.0	17.5
M1_0.437_3%SP_0.5%AWA		0.437		32.5	50.0	17.5
M1_0.46_3%SP_0.5%AWA		0.46		32.5	50.0	17.5
M1_0.39_3%SP_1%AWA	0.01	0.39	0.03	32.5	50.0	17.5
M1_0.40_3%SP_1%AWA		0.40		32.5	50.0	17.5
M1_0.41_3%SP_1%AWA		0.41		32.5	50.0	17.5
M1_0.42_3%SP_1%AWA		0.42		32.5	50.0	17.5
M1_0.437_3%SP_1%AWA		0.437		32.5	50.0	17.5
M1_0.46_3%SP_1%AWA		0.46		32.5	50.0	17.5
M1_0.39_3%SP_1.5%AWA	0.015	0.39	0.03	32.5	50.0	17.5
M1_0.40_3%SP_1.5%AWA		0.40		32.5	50.0	17.5
M1_0.41_3%SP_1.5%AWA		0.41		32.5	50.0	17.5
M1_0.42_3%SP_1.5%AWA		0.42		32.5	50.0	17.5
M1_0.437_3%SP_1.5%AWA		0.437		32.5	50.0	17.5
M1_0.46_3%SP_1.5%AWA		0.46		32.5	50.0	17.5

Dry powder constituents were first mixed together for 2 min at slow speed in a planetary mixer. After this step, water was added to dry mix. Then, the mixing phase consisted of four steps: 1 minute at slow speed,

followed by 3 minutes of mixing at high speed. After stopping the mixing, the bowl is scraped in order to homogenize the mortar. Lastly, the mixing was continued for 2 minutes at fast speed.

2.2. Yield stress measurement

Usually, the measurement of yield stress was carried out by rotational rheometry, especially using vane geometry [5,33,35–37]. In this study, the cone penetrometer was used. This type of measurement is easy to carry out and has been shown to be accurate for printable firm materials [38]. Also non-destructive static plate tests could have been used to monitor structural build-up but this technique requires larger quantities of material in order to obtain sufficient settlement to induce shear at the plate surface [39,40].

The standard BS ISO 13765-1:2004 characterises the use of the cone penetrometer [41]. Indeed, this test aims to determine the workability and the consistency of the mortar under a certain stress caused by the dropping cone (under gravity).

Firstly, the cement mortar is introduced in conical molds in two compacted layers (25 strokes per layer) in order to have a homogeneous material with limited entrapped void. The excess mortar is removed using a trowel or a spatula and the mold is placed under the dropping cone. Then, the testing machine is adjusted so that the tip of the cone is in contact with the surface sample. Finally, the cone is dropped during 5 seconds: it penetrates into the mortar sample under its own weight. The penetration depth is measured with accuracy of 0.01 mm. Measurements are replicated 5 times and the average value is taken into account. The dispersion of the measurements is also computed.

The yield stress of the materials is computed from the depth of penetration h of the standardized cone used in this study (tip angle of 30°, mass of 80 g). The yield stress computation comes from the force balance between gravity and friction on the cone surface:

$$\tau_0 = \frac{m \times g \times \cos^2\theta}{\pi h^2 \times \tan\theta} \quad (1)$$

Where h is the penetration depth (m), m the cone mass (kg) and g the gravity acceleration.

Roussel [18,19] has defined a structural build-up coefficient A_{thix} which models the constant rate of increase of the yield stress over resting time [18,42]:

$$\tau_0(t_{rest}) = \tau_{0,0} + A_{thix} t_{rest} \quad (2)$$

Where $\tau_{0,0}$ is the initial yield stress of the material and t_{rest} is the resting time.

Recently, Perrot and co-authors have shown that the Roussel model deviates from the yield stress evolution after one hour of rest [35,37]. They have developed a non-linear law that describes the yield stress exponential increase for longer resting time. In this model, the authors used a time parameter (t_c) that corresponds to the time when the yield stress increase becomes non-linear [35,37].

$$\tau_0(t_{rest}) = \tau_{0,0} + A_{thix} t_c \left(e^{t_{rest}/t_c} - 1\right) \quad (3)$$

In order to describe the yield stress evolution over resting time, cone penetration tests were carried out at regular intervals of 10 min on the same sample. The yield stress was measured at different resting times after the end of mixing (5, 15, 25, 35, 45, 55 and 65 minutes).

2.3. Measurement of material permeability at the fresh state

A mortar-dedicated device (Figure 1) developed by Picandet et al. [31] is used for the measurement of the permeability of the tested materials. This device allows to measure the volume of fluid flowing through the mortar submitted to pressure gradient. The steel cell containing the tested mortar is connected to air pressure inducing water head with a 1 kPa accuracy.

The mortar is placed on a filtration system which consists in 2 thin Fisherbrand® filter papers (thickness of 160 µm and mesh size of 8 µm) placed over a porous stone. This filtration system is saturated with water before testing. A perforated plate with filter paper covers the top of the sample for a homogeneous pressure repartition. About 250 ml of water is added over the sample to guaranty the water-saturation of the mortar during the whole test.

For the measurement of the mortar volume, the sample is weighted before the beginning of the test. Just after pouring the mortar, vibration is applied to minimize entrapped air. The sample height is measured, before the beginning and after the end of the test. This allows the computation of the mortar density and of the test-induced settlement due to pressure gradient application. Tests started 15 minutes after the contact between water and cement.

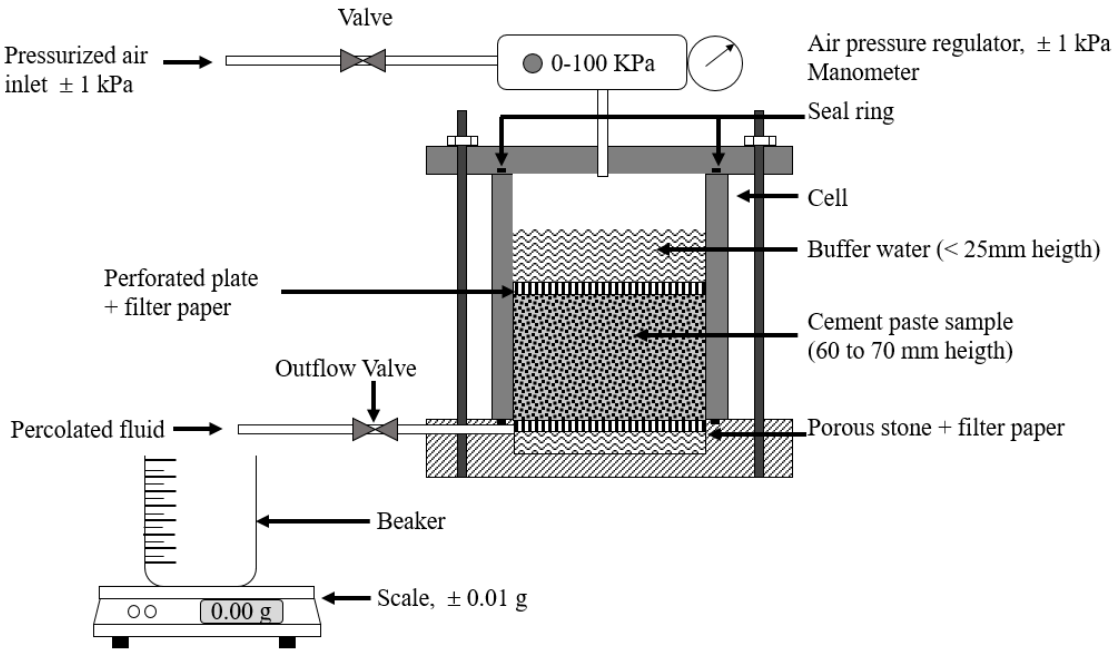

Fig. 1 : Permeability measurement device [31]

The permeability coefficient, k, is computed using Darcy's law (Eq. (1)):

$$k = Q \times \frac{h_i}{S \times \Delta H} \tag{4}$$

Where Q is the measure water flow rate measured with the scale (as shown in Figure 1), hi the sample height and ΔH is the water head.

At the beginning of the test, the water flow rate Q is maximal due to the consolidation of the tested material. Then, Q decreases to reach a plateau whose value is used in order to compute the permeability coefficient.

The consolidation also decreases the amount of water initially present in the mortar. This decrease in the water content is evaluated by measuring the material settlement.

2.4. Elastic modulus of fresh mortar

In order to measure the elastic modulus of fresh mortar, arheometer equipped with a plate geometry was used. The test consists in an unconfined one-dimensional compression of a mortar cylinder 38 mm high and 50 mm diameter. The sample was placed between two parallel plates. Constant rate of displacement protocol was performed at 1 mm/min. For each mortar three samples were tested. The test protocol consists of two cycles of loading and unloading. The first cycle is of the order of one-tenth of a millimeter in order to obtain a plane surface. The second cycle was performed to calculate the elastic modulus.

2.5. 3D concrete printer and printing parameters

The home-made 3D printer used in this study is a combination of a 6-axis robot (with a payload of 195 kg) with a Giema TP5 electric pump initially dedicated to rendering operations (pressure capacity: 20 bar – max flow rate: 40 l/min).

Tested mortar is prepared separately using a 100 litres concrete mixer and is then poured into the pump reservoir. A 6 m long, and 35 mm in diameter hose pipe is used to connect the pump reservoir to the nozzle mounted on the robot arm. Rectangular nozzle with the cross section of 21×40 mm² was used to extrude and deposit the mortar.

Different printing speeds (16, 18, 20 and 25 mm/s) were used to print the mortar in the water and only one speed (25 mm/s) was used to print it in the air, with a deposit height of 20 mm and a mortar flow rate of about 3 l/min (Figure 2). After 24 hours, the different specimens were kept in the containers with water at controlled environment (20 °C and 50% relative humidity) until testing.

In order to avoid material blockage in the hose pipes at startup and to facilitate pumping, a lubricant called slip (synthetic product or cement slurry W/C ratio between 0.5 and 0.8) was pumped before the mortar.

Fig. 2: Ongoing 3D printing of mortar –left: sample printed in air, right: sample printed in water.

2.6. Compressive strength of printed samples

In order to verify if the printed samples had compressive strength in accordance with expectations, compressive strength measurements were carried out; 76 mm high with a rectangular cross-section of 45x45 mm² were tested in compression using a 50 kN loading frame (constant rate of displacement of 1 mm/min).

For each printing speed, four specimens were tested and the averaged compressive strengths were then computed and compared.

The elastic modulus, E in GPa, was calculated using Eq. (2) in the linear part of the stress-strain curve:

$$E = \frac{\Delta\sigma}{\Delta\varepsilon} \quad (4)$$

Where σ and ε are respectively the axial stress and axial strain. The axial strain is computed by dividing the displacement by the initial height of the sample.

Before each compressive strength, samples are weighted and measured in order to compute their apparent densities.

3. Mix-design and fresh-state properties

3.1. Initial yield stress and Structural build-up rate

Figures 3 to 5 show the evolution of the yield stress in function of the resting time for the mortars for different W/C. Fitting of Roussel linear model [18,19] and Perrot et al. non-linear model [35] are also drawn in these figures.

It highlights that the increase of the yield stress of the tested cement mortar is almost linear during the first 45 min. In this period, the Roussel model accurately predict the structural build-up at rest. For longer resting period, the model developed by Perrot et better predicts the increase in yield stress [35]. It means that the A_{thix} coefficient, determined by Roussel model during the first 45 mincan be efficiently used to model the yield stress increase. All measured values of A_{thix} are plotted in Fig. 8 and Fig. 9.

Fitting parameters of both models are summarized in Table 2.

Table 2: Model parameters

		Roussel linear model (Roussel.2005)		Perrot et al. Exponentiel model (Perrot.2015)		
Formulations	E/C	Athix ($Pa.min^{-1}$)	$\tau_{0,0}$ (Pa)	Athix ($Pa.min^{-1}$)	$\tau_{0,0}$ (Pa)	t_c (min)
M1_0.38_3%SP	0.38	27.2	746.7	11.3	746.7	25.3
M1_0.39_3%SP	0.39	24.48	673.7	16.5	673.7	48.5
M1_0.40_3%SP	0.40	18.8	485.2	13.8	485.2	62.4
M1_0.39_3%SP_0.5%AWA	0.39	241.7	112.8	185.5	112.8	84.2
M1_0.40_3%SP_0.5%AWA	0.40	51.6	420.4	34.9	420.4	48.2
M1_0.41_3%SP_0.5%AWA	0.41	26.2	520.9	16.0	520.9	43.0
M1_0.42_3%SP_0.5%AWA	0.42	20.7	287.9	12.1	287.9	37.8
M1_0.39_3%SP_1%AWA	0.39	199.0	672.4	166.5	672.4	98.0
M1_0.40_3%SP_1%AWA	0.40	46.8	505.1	33.7	505.1	67.1
M1_0.41_3%SP_1%AWA	0.41	28.3	543.8	21.9	543.8	63.6
M1_0.42_3%SP_1%AWA	0.42	22.3	525.6	15.4	525.6	50.2
M1_0.39_3%SP_1.5%AWA	0.39	123.5	1142.4	107.3	1142.4	125.7
M1_0.40_3%SP_1.5%AWA	0.40	48.3	1089.3	38.9	1089.3	82.3
M1_0.41_3%SP_1.5%AWA	0.41	29.6	634.1	22.2	634.1	67.0

M1_0.42_3%SP_1.5%AWA	0.42	13.4	452.1	9.6	452.1	58.5

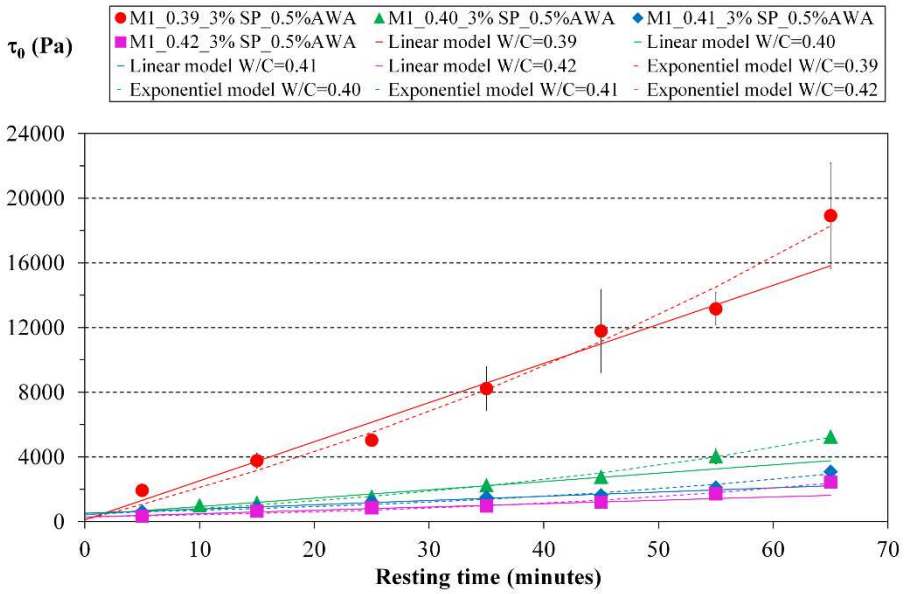

214

215 **Fig. 3: Evolution of the yield stress vs resting time for the materials for different W/C and 0.5% of AWA.**
216 **Comparison of the experimental data with prediction of the Perrot et al. [35] and Roussel models [19]**

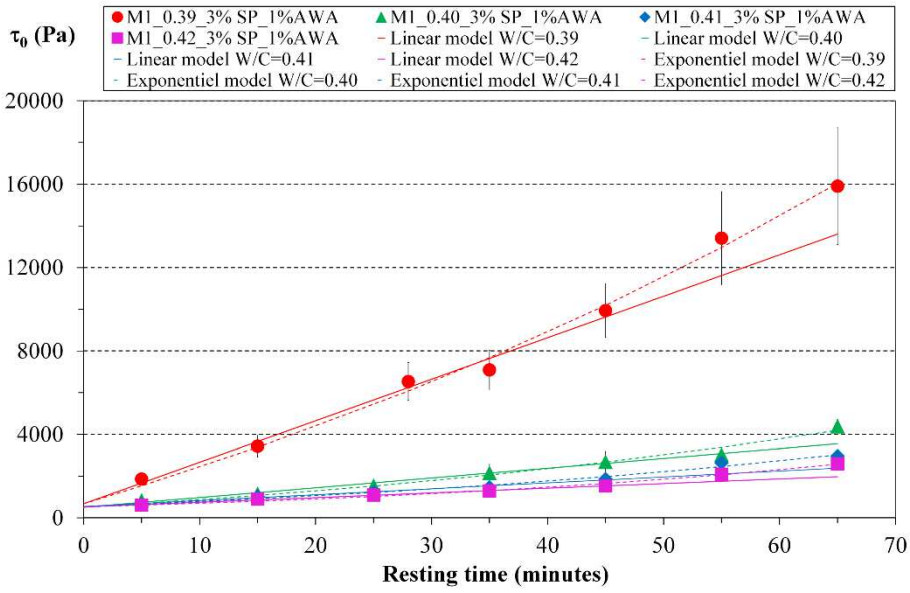

217

218 **Fig. 4: Evolution of the yield stress versus resting time for the materials for different W/C and 1% of AWA.**
219 **Comparison of the experimental data with prediction of the Perrot et al. [35] and Roussel models [19]**

220

221

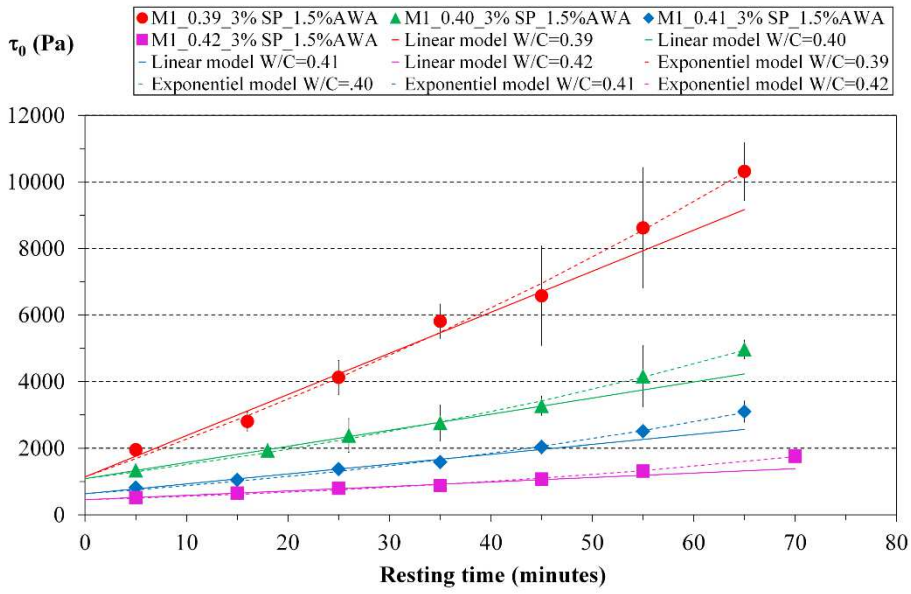

222

223 **Fig.5: Evolution of the yield stress vs resting time for the materials for different W/C and 1.5% of AWA.**
224 **Comparison of the experimental data with prediction of the Perrot et al. [35] and Roussel models [19]**

225

226 The effect of W/C on the structural build-up rate of cement mortar with various AWA dosages is shown in
227 Figure 6. The effects of AWA dosage on structural build-up rate of cement mortar with various W/C are
228 shown in Figure 7.

229 We first observe that the structural build-up rate decreases when the water to cement ratio is increased.
230 Indeed, when the water to cement ratio varies from 0.39 to 0.42, the structural build-up rate decreases by
231 91–89% depending on the dosage of AWA.

232 The mortar without AWA shows a less significant decrease of structural build-up rate with W/C ratio.
233 Indeed, it decreases by 28% when water to cement ratio varies from 0.38 to 0.40.

234 For higher W/C, the effects of W/C on the structural build-up rate were not highly significant, as shown in
235 Figure 6. It became more influencing at lower W/C. This is in agreement with prediction of Yodel model:
236 the yield stress and structural build-up variation are larger when apporaching the packing fraction [43,44].

On the other hand, the structural build-up rate was more sensitive to AWA dosage in lower W/C than in higher W/C, as shown in Figure 7.

The addition of water reduces the solids concentration, resulting in less resistance to flow. Workability is improved with increasing water-to-cementitious materials ratios up to a certain point, after which bleeding and segregation can become a problem [45].

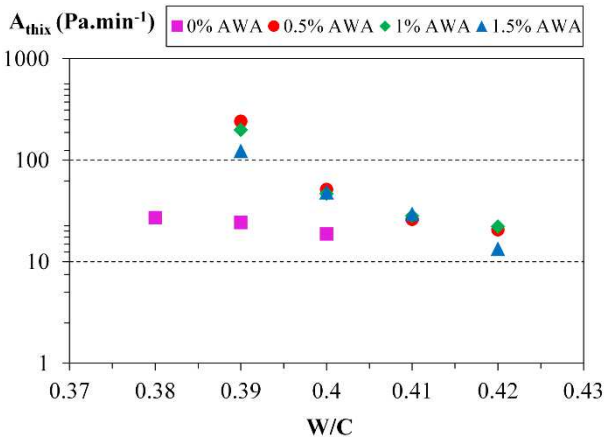

Fig. 6: Evolution of the structural build-up rate versus the W/C ratio of cement mortar with various AWA contents.

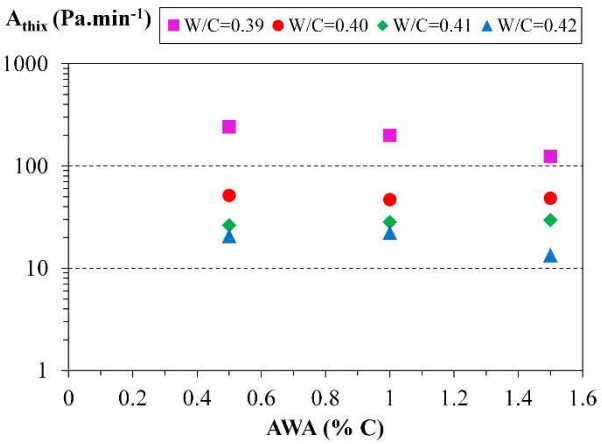

Fig. 7: Evolution of the structural build-up rate versus the AWA contents of cement mortar with various W/C ratio.

3.2. Permeability

The variation of fresh mortar permeability as a function of water to cement ratio is shown in Figure 8. Wathever the AWA content, the permebality of fresh mortar increases with W/C. It can be explained by the increase of the void ratio and porosity [33] that are both closely linked to W/C [31]. Therefore, mortars with high W/C have higher porosity causing the acceleratation of water flow through the tested specimen.

For constant W/C, the permeability decreases with increase in AWA content. For exemple, for the mortar with W/C equal to 0.42, an augmentation in the dosage of AWA from 0% to 0.5%, 1% and 1.5% resulted an decease of permeability for 88%, 94% and 98% respectively. This can be explained by the increase in the interstitial liquid phase viscosity and by changes in the cement grain assembly. In fact, this is due to the mode of function of the AWA polymers bonds together, thus adsorbing and fixing part of the mixing water inside an gel [46,47]. A three-dimensional gel structure is created thanks to van der Waals forces and hydrogen bonds increasing the viscosity of the interstitial phase and thus reducing permeability [48].

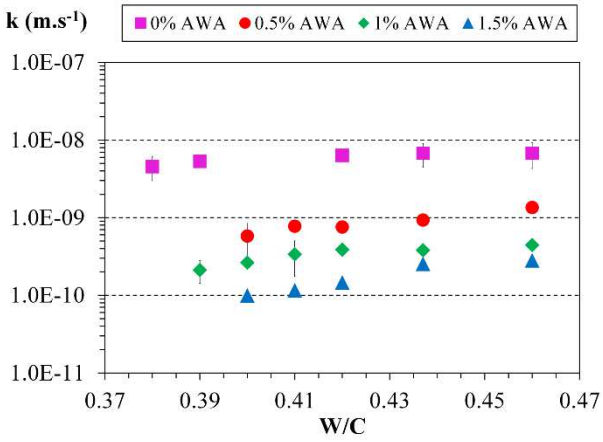

Fig. 8: Permeability coefficient k ($m.s^{-1}$) vs W/C for various AWA contents.

3.3. Fresh mortar elastic modulus

Concrete 3D printing carried out with the extrusion/deposit method can be seen as a multistep process. The material has to be transported (often by pumping) before its deposit when the material leaves the extruder.

Once deposited, the material has to form a structure that remains stable over the whole printing process. Then, the specification sheet for the behaviour of the freshly mixed material has to comply with all the requirements defined at each step of the process. Such specifications lead to draw a mix-design window that may need compromise between fluidity and strength or between fast structural build-up and long workable time.

Figure 9 shows the effect AWA content on fresh mortar elastic modulus. We can observe that, over a critical AWA content the elastic modulus of fresh mortar decreases with increasing the AWA content at a same value of yield stress. This means that the AWA increase will lower the critical strain but increase the elastic deformation. Further studies will be needed to accurately understand the mechanisms explaining this result at the microscale.

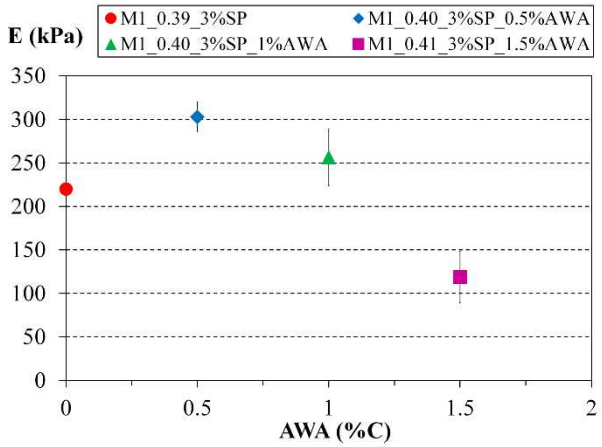

Fig. 9: Effect of AWA content on fresh mortar elastic modulus.

3.4. Optimized mix-design

Rheological requirements of for 3D printing are dictated by the pumping stage, the extrusion/deposition stage and finally by the overall stability of the structure during printing.

In this study, the pump presents a pressure capacity of 20 bar and the hose pipe is 6 m long with an inner diameter of 35 mm. Preliminary pumping tests have allowed to validate that the shear yield stress of the

material must remain under 1.1 kPa in order to keep the pressure under the pump pressure capacity. To maintain a safety margin during pumping, the water content of the material was adjusted in order to obtain hear yield stress of 0.8 kPa for the printing test. For the mortar without AWA the W/C is equal to 0.39, for the mortar with 0.5% and 1% of AWA the W/C is equal to 0.40 and for the mortar with 1.5% of AWA the W/C ratio is equal to 0.41 respectively.

Also, in order to ensure that the printed structure remains stable, the material must build-up as fast as possible and must present the highest possible elastic modulus. this last property is considered to be detrimental for 3D printing because low elastic modulus can lead to self-buckling. As previously exposed, highest structural build-up rate and highest elastic modulus are found at a AWA dosage of 0.5%. In order to ensure the 3D printing wall stability during the process, the yield stress and the elastic modulus of the first deposited layer that undergoes the heaviest load must be sufficient to sustain this load and to keep its shape. Therefore, AWA dosage of 0.5% (overall stability requirements) and W/C of 0.39 (in order to have a yield stress of 0.8 kPa for pumpability) were chosen in order to perform the underwater printing.

It is also worth noting that the dosage of 0.5% of AWA is sufficient to significantly decrease the permeability of the mortar hence enhancing its anti-washout properties, as shown in Figure 8. Indeed, from 0 to 0.5% of AWA allows to decrease the permeability of the mortar by around one order of magnitude whereas from 0.5 to 1% divide only by 2 the permeability.

4. Underwater printing 3D printing materials

It is important to note that the nozzle displacement velocity (printing speed in our study) can signicantly affect the behaviour the printed material. This is even more pronounced in the case of concrete printing due to the presence of larger particles in comparison with the printing of other types of materials [49,50]. It is expected that a balance can be found between pumping flow rate and nozzle velocity leading to an optimal printing speed [32]. For the printed mortar, it has been noted that with a constant pump flow, the increase in print speed reduces the width of the printed mortar.

306 The mechanical properties measured in this study are summarized in Table 3. Compressive strength of the
307 mortar samples printed in water is plotted as a function of printing speed in Figure 10. For the studied
308 materials, the compressive strength decreases with the studied printing speed. Results shows that the
309 compressive strength decreases by 10.4% when the printing speed varies from 16 to 25 $mm.s^{-1}$. This is
310 decrease can be explained by both size effect and strain gradients within the cross section of the filaments
311 of mortar, caused by the differences between mortar velocity in the printhead and nozzle displacement
312 velocity [51]. This may cause what can be called under or over-extrusion and leads to a decrease of the
313 sample density.

314 In contrast to compressive strength, elastic modulus displays a different trend. Figure 11shows that below
315 a critical printing speed, the elastic modulus of 3D printable mortar decreased with increasing the printing
316 speed. A too fast nozzle displacement may have led to tensile stresses in the filament cross section that may
317 have led to material micro-failure or fracture that may significantly affect the mechanical properties of the
318 sample once hardened [49].

319 If we compare the mechanical properties obtained with the 3D printable mortar specimens in water with
320 those printed in the air, we observe a decrease of 7% and 11% respectivly for compressive strength and
321 elastic modulus. This can be explained by washout effect at the surface of the layers.

322 **Table 3 : Densities and mechanical properties of printed samples.**

	Printing speed ($mm.s^{-1}$)	Density ($kg.m^{-3}$)	Compressive strength (MPa)	Elastic modulus (GPa)
Water	16	2280 ±25	37.84 ± 6.77	2.59 ± 0.46
	18	2280 ± 20	37.06 ± 6.01	3.42 ± 0.43
	20	2260 ± 24	35.49 ± 2.68	2.86 ± 0.18
	25	2240 ± 18	33.90 ± 10.84	2.52 ± 1.18
Air	25	2270 ± 32	36.45 ± 3.09	2.82 ± 0.48

323

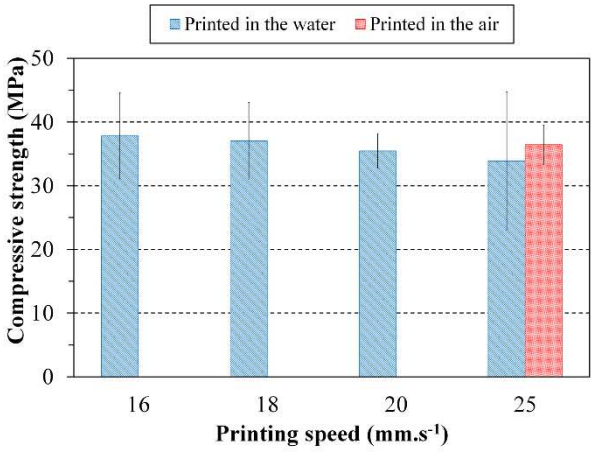

324

325 **Fig. 10: Evolution of the compressive strength of 3D printable cement mortar versus the printing speed.**

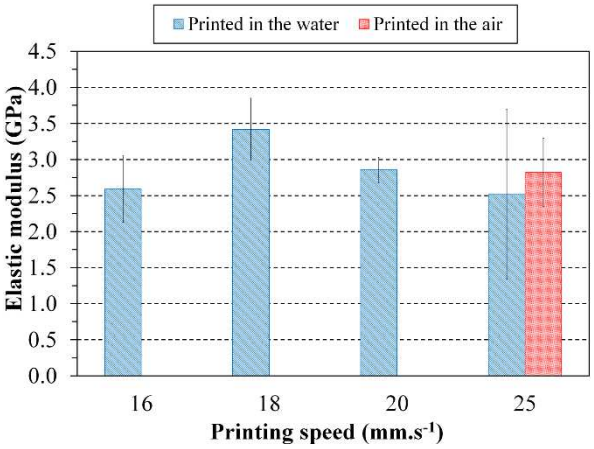

326

327 **Fig. 11: Evolution of the elastic modulus of 3D printable cement mortar versus the printing speed.**

328 Cut section of sample printed in water at different speed is shown in Figure 12. It is worth noting the absence
329 of cold joints and adhesion defects between the extruded layers for printing speed of 18 and 20 mm/s. This
330 means that at these printing speeds, water does not alter adhesion between layers.

331 However, it can be seen of Fig. 12c that some voids appear between layers. It can be attributed to under-
332 extrusion: the nozzle moves to fast and creates tension in the deposited layer leading to void formation.
333 Such results is in agreement with the measured densities presented in table 3.

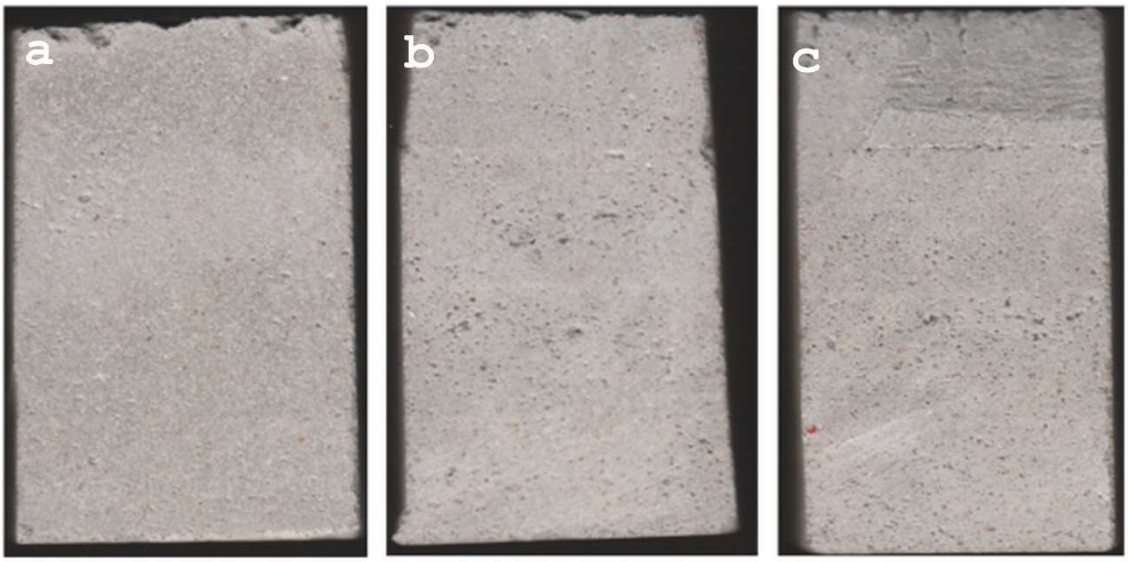

Fig.12: Cut section of printed samples in water: a) printed with a speed of 18 mm.s-1 - b) printed with a speed of 20 mm.s-1 - c) printed with a speed of 25 mm.s-1

5. Conclusion

This study aimed to investigate the possibility of producing an underwater 3D printing material and highlights the effect of printing speed on mechanical properties. Firstly, the effects of W/C and AWA content on the fresh properties were studied, with the goal of designing a printable mortar.

Tested mortars were characterised by measuring their yield stress, structural build-up rate, water permeability and elastic modulus. Literature has shown that their properties are involved during the printing process and need to be fine-tuned for the successful implementation of the underwater 3D printing of mortar. The experimental results show that he structural build-up rate is influenced by the AWA content and W/C. In fact, the structural build-up rate decreases with the increase in W/C and AWA content.

Moreover, the addition of AWA decreases the permeability of the fresh mortar. This can be explained by increase in the interstitial fluid viscosity and by densification of the particle network.

After selection of the best formulation, mortar 3D printing has been performed at different printing speed (nozzle displacement velocity) and the compressive strength of the printed samples have been measured.

Finally, for the underwater 3D printing materials, the compressive strength decreases with the increase of printing speed. In contrast to compressive strength, elastic modulus shows quite a different trend, below a critical printing speed the elastic modulus of 3D printable mortar decreases with increasing the printing speed.

6. Aknowledgement

The authors want to thank the "Pôle Homme Mer Littoral" of Université Bretagne Sud for funding this research program.

7. References

[1] B. Khoshnevis, Automated construction by contour crafting—related robotics and information technologies, Autom. Constr. 13 (2004) 5–19. doi:10.1016/j.autcon.2003.08.012.

[2] B. Khoshnevis, D. Hwang, K.T. Yao, Z. Yeh, Mega-scale fabrication by Contour Crafting, Int. J. Ind. Syst. Eng. 1 (2006) 301. doi:10.1504/IJISE.2006.009791.

[3] T.T. Le, S.A. Austin, S. Lim, R.A. Buswell, A.G.F. Gibb, T. Thorpe, Mix design and fresh properties for high-performance printing concrete, Mater. Struct. 45 (2012) 1221–1232. doi:10.1617/s11527-012-9828-z.

[4] S. Lim, R.A. Buswell, T.T. Le, S.A. Austin, A.G.F. Gibb, T. Thorpe, Developments in construction-scale additive manufacturing processes, Autom. Constr. 21 (2012) 262–268. doi:10.1016/j.autcon.2011.06.010.

[5] A. Perrot, D. Rangeard, A. Pierre, Structural built-up of cement-based materials used for 3D-printing extrusion techniques, Mater. Struct. 49 (2016) 1213–1220. doi:10.1617/s11527-015-0571-0.

[6] R.A. Buswell, R.C. Soar, A.G.F. Gibb, A. Thorpe, Freeform Construction: Mega-scale Rapid Manufacturing for construction, Autom. Constr. 16 (2007) 224–231. doi:10.1016/j.autcon.2006.05.002.

[7] B. Nematollahi, M. Xia, J. Sanjayan, Current Progress of 3D Concrete Printing Technologies, in: 2017. doi:10.22260/ISARC2017/0035.

[8] C. Gosselin, R. Duballet, P. Roux, N. Gaudillière, J. Dirrenberger, P. Morel, Large-scale 3D printing of ultra-high performance concrete – a new processing route for architects and builders, Mater. Des. 100 (2016) 102–109. doi:10.1016/j.matdes.2016.03.097.

[9] T. Wangler, E. Lloret, L. Reiter, N. Hack, F. Gramazio, M. Kohler, M. Bernhard, B. Dillenburger, J. Buchli, N. Roussel, R. Flatt, Digital Concrete: Opportunities and Challenges, RILEM Tech. Lett. 1 (2016) 67. doi:10.21809/rilemtechlett.2016.16.

[10] A. Perrot, D. Rangeard, E. Courteille, 3D printing of earth-based materials: Processing aspects, Constr. Build. Mater. 172 (2018) 670–676. doi:10.1016/j.conbuildmat.2018.04.017.

[11] S. Amziane, Setting time determination of cementitious materials based on measurements of the hydraulic pressure variations, Cem. Concr. Res. 36 (2006) 295–304. doi:10.1016/j.cemconres.2005.06.013.

[12] S. Amziane, C.F. Ferraris, Cementitious paste setting using rheological and pressure measurements, ACI Mater. J. 104 (2007) 137.

[13] P.H. Billberg, N. Roussel, S. Amziane, M. Beitzel, G. Charitou, B. Freund, J.N. Gardner, G. Grampeix, C.-A. Graubner, L. Keller, K.H. Khayat, D.A. Lange, A.F. Omran, A. Perrot, T. Proske, R. Quattrociocchi, Y. Vanhove, Field validation of models for predicting lateral form pressure exerted by {SCC}, Cem. Concr. Compos. 54 (2014) 70–79. doi:http://dx.doi.org/10.1016/j.cemconcomp.2014.02.003.

[14] A. Perrot, S. Amziane, G. Ovarlez, N. Roussel, {SCC} formwork pressure: Influence of steel rebars, Cem. Concr. Res. 39 (2009) 524–528. doi:http://dx.doi.org/10.1016/j.cemconres.2009.03.002.

[15] G. Ovarlez, N. Roussel, A Physical Model for the Prediction of Lateral Stress Exerted by Self-Compacting Concrete on Formwork, Mater. Struct. 39 (2006) 269–279. doi:10.1617/s11527-005-9052-1.

[16] N. Roussel, F. Cussigh, Distinct-layer casting of SCC: The mechanical consequences of thixotropy, Cem. Concr. Res. 38 (2008) 624–632. doi:10.1016/j.cemconres.2007.09.023.

[17] E. Lloret, A.R. Shahab, M. Linus, R.J. Flatt, F. Gramazio, M. Kohler, S. Langenberg, Complex concrete structures: Merging existing casting techniques with digital fabrication, Comput.-Aided Des. 60 (2015) 40–49. doi:10.1016/j.cad.2014.02.011.

[18] N. Roussel, Steady and transient flow behaviour of fresh cement pastes, Cem. Concr. Res. 35 (2005) 1656–1664. doi:10.1016/j.cemconres.2004.08.001.

[19] N. Roussel, A thixotropy model for fresh fluid concretes: Theory, validation and applications, Cem. Concr. Res. 36 (2006) 1797–1806. doi:10.1016/j.cemconres.2006.05.025.

[20] N. Roussel, Rheological requirements for printable concretes, Cem. Concr. Res. 112 (2018) 76–85. doi:10.1016/j.cemconres.2018.04.005.

[21] D. Lowke, T. Kränkel, C. Gehlen, P. Schießl, Effect of Cement on Superplasticizer Adsorption, Yield Stress, Thixotropy and Segregation Resistance, in: K.H. Khayat, D. Feys (Eds.), Des. Prod. Place. Self-Consol. Concr., Springer Netherlands, Dordrecht, 2010: pp. 91–101. doi:10.1007/978-90-481-9664-7_8.

[22] R. Ferron, A. Gregori, Z. Sun, S.P. Shah, Rheological Method to Evaluate Structural Buildup in Self-Consolidating Concrete Cement Pastes, ACI Mater. J. 104 (2007). doi:10.14359/18669.

[23] N. Roussel, G. Ovarlez, S. Garrault, C. Brumaud, The origins of thixotropy of fresh cement pastes, Cem. Concr. Res. 42 (2012) 148–157. doi:10.1016/j.cemconres.2011.09.004.

[24] F.P. Bos, Z.Y. Ahmed, R.J.M. Wolfs, T.A.M. Salet, 3D Printing Concrete with Reinforcement, in: D.A. Hordijk, M. Luković (Eds.), High Tech Concr. Technol. Eng. Meet, Springer International Publishing, Cham, 2018: pp. 2484–2493. doi:10.1007/978-3-319-59471-2_283.

[25] K.H. Khayat, M. Sonebi, Effect of mixture composition on washout resistance of highly flowable underwater concrete, Mater. J. 98 (2001) 289–295.

[26] M. Sonebi, K.H. Khayat, Effect of mixture composition on relative strength of highly flowable underwater concrete, Mater. J. 98 (2001) 233–239.

[27] J.J. Assaad, C.A. Issa, Mechanisms of strength loss in underwater concrete, Mater. Struct. 46 (2013) 1613–1629. doi:10.1617/s11527-012-0004-2.

[28] N. Roussel, A. Lemaître, R.J. Flatt, P. Coussot, Steady state flow of cement suspensions: A micromechanical state of the art, Cem. Concr. Res. 40 (2010) 77–84. doi:10.1016/j.cemconres.2009.08.026.

[29] N. Massoussi, E. Keita, N. Roussel, The heterogeneous nature of bleeding in cement pastes, Cem. Concr. Res. 95 (2017) 108–116.

[30] A. Perrot, T. Lecompte, H. Khelifi, C. Brumaud, J. Hot, N. Roussel, Yield stress and bleeding of fresh cement pastes, Cem. Concr. Res. 42 (2012) 937–944. doi:http://dx.doi.org/10.1016/j.cemconres.2012.03.015.

[31] V. Picandet, D. Rangeard, A. Perrot, T. Lecompte, Permeability measurement of fresh cement paste, Cem. Concr. Res. 41 (2011) 330–338. doi:10.1016/j.cemconres.2010.11.019.

[32] A. Perrot, D. Rangeard, V. Picandet, S. Serhal, Effect of coarse particle volume fraction on the hydraulic conductivity of fresh cement based material, Mater. Struct. 48 (2015) 2291–2297. doi:10.1617/s11527-014-0311-x.

[33] A. Perrot, D. Rangeard, V. Picandet, Y. Mélinge, Hydro-mechanical properties of fresh cement pastes containing polycarboxylate superplasticizer, Cem. Concr. Res. 53 (2013) 221–228. doi:10.1016/j.cemconres.2013.06.015.

[34] A. Pierre, A. Perrot, V. Picandet, Y. Guevel, Cellulose ethers and cement paste permeability, Cem. Concr. Res. 72 (2015) 117–127. doi:10.1016/j.cemconres.2015.02.013.

[35] A. Perrot, A. Pierre, S. Vitaloni, V. Picandet, Prediction of lateral form pressure exerted by concrete at low casting rates, Mater. Struct. 48 (2015) 2315–2322. doi:10.1617/s11527-014-0313-8.

[36] F. Mahaut, S. Mokéddem, X. Chateau, N. Roussel, G. Ovarlez, Effect of coarse particle volume fraction on the yield stress and thixotropy of cementitious materials, Cem. Concr. Res. 38 (2008) 1276–1285. doi:10.1016/j.cemconres.2008.06.001.

[37] T. Lecompte, A. Perrot, Non-linear modeling of yield stress increase due to SCC structural build-up at rest, Cem. Concr. Res. 92 (2017) 92–97. doi:10.1016/j.cemconres.2016.11.020.

[38] D. Lootens, P. Jousset, L. Martinie, N. Roussel, R.J. Flatt, Yield stress during setting of cement pastes from penetration tests, Cem. Concr. Res. 39 (2009) 401–408. doi:10.1016/j.cemconres.2009.01.012.

[39] H. Sleiman, A. Perrot, S. Amziane, A new look at the measurement of cementitious paste setting by Vicat test, Cem. Concr. Res. 40 (2010) 681–686. doi:http://dx.doi.org/10.1016/j.cemconres.2009.12.001.

[40] S. Amziane, A. Perrot, The plate test carried out on fresh cement-based materials:How and why?, Cem. Concr. Res. 93 (2017) 1–7. doi:10.1016/j.cemconres.2016.12.002.

[41] BS ISO 13765-1:2004, Refractory mortars. Determination of consistency using the penetrating cone method, (2006).

[42] L. Josserand, O. Coussy, F. de Larrard, Bleeding of concrete as an ageing consolidation process, Cem. Concr. Res. 36 (2006) 1603–1608. doi:10.1016/j.cemconres.2004.10.006.

[43] R.J. Flatt, P. Bowen, Yield stress of multimodal powder suspensions: an extension of the YODEL (Yield Stress mODEL), J. Am. Ceram. Soc. 90 (2007) 1038–1044.

[44] R.J. Flatt, P. Bowen, Yodel: a yield stress model for suspensions, J. Am. Ceram. Soc. 89 (2006) 1244–1256.

[45] L. Shen, L. Struble, D. Lange, Modeling static segregation of self-consolidating concrete, ACI Mater. J. 106 (2009) 367–374.

[46] K.H. Khayat, Viscosity-enhancing admixtures for cement-based materials—an overview, Cem. Concr. Compos. 20 (1998) 171–188.

[47] L. Patural, P. Marchal, A. Govin, P. Grosseau, B. Ruot, O. Deves, Cellulose ethers influence on water retention and consistency in cement-based mortars, Cem. Concr. Res. 41 (2011) 46–55.

[48] A. Pierre, A. Perrot, V. Picandet, Y. Guevel, Cellulose ethers and cement paste permeability, Cem. Concr. Res. 72 (2015) 117–127.

[49] B. Panda, S.C. Paul, N.A.N. Mohamed, Y.W.D. Tay, M.J. Tan, Measurement of tensile bond strength of 3D printed geopolymer mortar, Measurement. 113 (2018) 108–116. doi:10.1016/j.measurement.2017.08.051.

[50] O. Lužanin, D. Movrin, M. Plančak, Experimental investigation of extrusion speed and temperature effects on arithmetic mean surface roughness in FDM built specimens, J. Technol. Plast. 38 (2013) 179–190.

[51] F. Bos, R. Wolfs, Z. Ahmed, T. Salet, Additive manufacturing of concrete in construction: potentials and challenges of 3D concrete printing, Virtual Phys. Prototyp. 11 (2016) 209–225. doi:10.1080/17452759.2016.1209867.